A Hu Invariant as a Shape Circularity Measure

Joviša Žunić, [a, *] Kaoru Hirota,[b] Paul L. Rosin[c]

[a] Department of Computer Science, University of Exeter, Harrison Building, Exeter EX4 4QF, U.K.
e-mail: J.Zunic@ex.ac.uk

[b] Department of Computational Intelligence and Systems Science, Graduate School of Science and Engineering, Tokyo Institute of Technology, G3-49, 4259 Nagatsuta, Modori-ku, Yokohama 226-8502, Japan.
e-mail: hirota@hrt.dis.titech.ac.jp

[c] School of Computer Science, Cardiff University, Cardiff CF24 3AA, Wales, U.K.
e-mail: Paul.Rosin@cs.cf.ac.uk

[*] J. Žunić is also with the Mathematical Institute, Serbian Academy of Arts and Sciences, Belgrade.

Abstract

In this paper we propose a new circularity measure which defines the degree to which a shape differs from a perfect circle. The new measure is easy to compute and being area based, is robust – e.g., with respect to noise or narrow intrusions. Also, it satisfies the following desirable properties:
– it ranges over $(0, 1]$ and gives the measured circularity equal to 1 if and only if the measured shape is a circle;
– it is invariant with respect to translations, rotations and scaling.

Compared with the most standard circularity measure, which considers the relation between the shape area and the shape perimeter, the new measure performs better in the case of shapes with boundary defects (which lead to a large increase in perimeter) and in the case of compound shapes. In contrast to the standard circularity measure, the new measure depends on the mutual position of the components inside a compound shape.

Also, the new measure performs consistently in the case of shapes with very small (i.e., close to zero) measured circularity. It turns out that such a property enables the new measure to measure the linearity of shapes.

In addition, we propose a generalization of the new measure so that shape circularity can be computed while controlling the impact of the relative position of points inside the shape. An additional advantage of the generalized measure is that it can be used for detecting small irregularities in nearly circular shapes damaged by noise or during an extraction process in a particular image processing task.

Keywords: shape, circularity measure, moments, Hu moment invariants, image processing.

1 Introduction

Shape descriptors are a powerful tool for shape classification tasks. Many shape descriptors have already been studied in the literature and applied in practice. Some examples are: elongation [32], convexity [21], rectangularity [24], rectilinearity [36], sigmoidality [25], orientability [38], etc. Note also that, due to the diversity of shapes and the diversity of applications in different areas such as computer science, medicine, biology, robotics, etc., several methods are often developed for measuring the same shape property. As an illustration we list just a few known methods for measuring shape convexity: [1, 11, 19, 21, 26, 37] and for computing the orientation of a shape: [3, 8, 13, 27, 28, 33]. The latter is often used within a shape normalisation procedure that is sometimes required prior to further shape analysis. All the methods developed have their strengths and weaknesses, and their suitability cannot be evaluated without knowing the particular application for which they are to be applied. Similar considerations hold for the other shape descriptors as well, including the circularity measure that will be considered here.

In this paper we define a new measure for circularity (circularity is sometimes referred to as *compactness* in the literature). Being one of the basic shape properties, circularity has already been extensively studied, and several methods for measuring the circularity already exist in the literature [4, 9, 12, 15, 20, 30]. Let us mention that $3D$-compactness and circularity in a discrete space have also been considered [2], but were defined in a different way. Probably the most standard circularity measure is derived from the relation between the shape area and the shape perimeter [29]. Taking into account that, among all shapes with the same area, the circle has the minimal perimeter, a circularity measure can be defined as

$$\mathcal{C}_{st}(S) = \frac{4 \cdot \pi \cdot area\_of\_S}{(perimeter\_of\_S)^2}. \tag{1}$$

It is easy to check that the following natural requirements, for such a defined circularity measure, hold:

(a) $\mathcal{C}_{st}(S) \in (0, 1]$;

(b) $\mathcal{C}_{st}(S) = 1$ if and only if S is a circle;

(c) $\mathcal{C}_{st}(S)$ is invariant with respect to similarity transformations (i.e., translations, rotations and scaling);

(d) For each $\delta > 0$ there is a shape S such that $0 < \mathcal{C}_{st}(S) < \delta$, i.e. there are shapes whose measured circularities are arbitrarily close to 0.

As mentioned, there are also other possibilities for defining a circularity measure. One of the general approaches to defining shape descriptor measures could also be applied to defining circularity. For example, let us fit a circle C to a measured shape S, then the circularity of the shape S can be estimated by comparing C and S. One straightforward possibility for a fitted circle C is the circle whose centroid coincides with the centroid of S and whose area is equal to the area of S. Finally, a circularity measure (i.e. the comparison between S and C) can be given as $\frac{area\_of\_(S \cap C)}{area\_of\_(S \cup C)}$. Of course, there are other variations of this approach.

Geometric moments will be used in the definition of the new circularity measure. It is worth mentioning that geometric moments are widely used in computer vision, image analysis, or pattern recognition tasks – see [29] or [10, 18, 27, 33] for more specific tasks. The (p, q)-*moment* $m_{p,q}(S)$ of a planar shape S is defined by the following:

$$m_{p,q}(S) \quad = \quad \iint_S x^p y^q \, dx \, dy$$

and has order $p + q$. Basic shape features (e.g., size, position, orientation, elongation) are computed from the moments having order less than or equal to two. E.g., $m_{0,0}(S)$ equals the area of S while $\left(\frac{m_{1,0}(S)}{m_{0,0}(S)}, \frac{m_{0,1}(S)}{m_{0,0}(S)}\right)$ is the centroid of S. Higher order moments are needed for computing, for example, the orientation of rotationally symmetric shapes [33] or moment invariants [10].

The *centralised* (p, q)-*moment* $\mu_{p,q}(S)$ of a planar set S is:

$$\mu_{p,q}(S) \;=\; \iint_S \left(x - \frac{m_{1,0}(S)}{m_{0,0}(S)}\right)^p \left(y - \frac{m_{0,1}(S)}{m_{0,0}(S)}\right)^q dxdy.$$

Of course, if the centroid of S and the origin coincide then $m_{p,q}(S) = \mu_{p,q}(S)$ for all p and q. Trivially, $m_{0,0}(S) = \mu_{0,0}(S)$, but in the rest of the paper we will use $\mu_{p,q}(S)$, rather than $m_{0,0}(S)$, for the area of S.

In this paper we show that the quantity

$$\mathcal{C}(S) = \frac{(\mu_{0,0}(S))^2}{2\pi \cdot (\mu_{2,0}(S) + \mu_{0,2}(S))}$$

can be used as a circularity measure. We show that the basic requirements **(a)**,**(b)**,**(c)** and **(d)** (given above) are also satisfied by $\mathcal{C}(S)$. Several given examples demonstrate the behaviour of the new measure. Also, we give a generalisation of the new measure in order to enable control of the impact of the points' positions inside the measured shape to the computed circularity.

Note that the quantity $(\mu_{2,0}(S) + \mu_{0,2}(S))/(\mu_{0,0}(S))^2$ is well known from the literature. It is one of the famous Hu moment invariants [10] (invariant to translation, rotation and scaling). The same quantity also appears as one of the geometric invariants derived in [35]. It is worth mentioning that moment invariants have been used in many classification tasks, but also some of them are used to measure shape properties. For example [24] uses the projective invariant $I_1(S) = (\mu_{2,0}(S) \cdot \mu_{0,2}(S) - (\mu_{1,1}(S))^2)/(\mu_{0,0}(S))^2$ (see [7]) to define an ellipticity measure, under the argument that any ellipse can be obtained by applying an affine transformation to a circle. More precisely, the ellipticity measure of a given shape S is obtained by comparing $I_1(S)$ with $\dfrac{1}{16\pi^2} = I_1(circle)$. The same paper derives a triangularity measure by the same reasoning and by using $I_1(S)$ again.

Such defined ellipticity and triangularity measures are adopted to range over $[0, 1]$ and peak at 1 for a perfect ellipse (or a perfect triangle). The problem is that for both measures, if the measured ellipticity (triangularity) equals 1 it is not guaranteed (or at least not proven) that the measured shape is a perfect ellipse (triangle). The circularity measure described here does not have such a disadvantage – it equals 1 if and only if the measured shape is a perfect circle.

The paper is organised as follows. The next section introduces the new circularity measure and proves several desirable properties of it. Section 3 gives some illustrative examples that demonstrate the behaviour of the new measure $\mathcal{C}(S)$ and compare it with the behaviour of the standard circularity measure $\mathcal{C}_{st}(S)$. In Section 4 we introduce a modification of $\mathcal{C}(S)$ which gives different weights to the points inside the shape depending on their position with respect to the measured shape centroid. In such a way, the impact on the computed circularity of the positions of points inside the shape can be controlled. Illustrative examples and theoretical consideration of the modified measure are also given. In Section 5 we discuss and demonstrate the suitability of a use of the new circularity measure for measuring shape linearity. Section 6 uses the circularity measure for a variety of image processing applications. Comments and conclusion are in the last section.

2 New Circularity Measure

In this section we define a new circularity measure. Through the paper we assume that all shapes considered are planar and compact (a closed and bounded set is said to be compact), even if this is not explicitly stated. Obviously, this is not a restriction in image processing tasks. We start with the quantity $(\mu_{2,0}(S) + \mu_{0,2}(S)/(\mu_{0,0}(S))^2$ and show that it reaches the

minimum value of $1/(2\pi)$ if and only if S is a circle. Exploiting this fact we will come to a new circularity measure. First, we prove the following theorem.

Theorem 1 *Let S be a given planar compact shape. Then*

$$\frac{\mu_{2,0}(S)+\mu_{0,2}(S)}{\mu_{0,0}(S)^2} \geq \frac{1}{2\pi}, \tag{2}$$

$$\frac{\mu_{2,0}(S)+\mu_{0,2}(S)}{\mu_{0,0}(S)^2} = \frac{1}{2\pi} \quad \Leftrightarrow \quad S \ \textit{is a circle.} \tag{3}$$

Proof. Let S be a given planar compact shape whose centroid coincides with the origin. Also, let C be the circle with radius $r=\sqrt{\mu_{0,0}(S)/\pi}$ (i.e. the areas of C and S are the same) and centred at the origin. Trivially:

(i) The areas of the set differences $S \setminus C$ and $C \setminus S$ are the same (because the areas of S and C are the same);

(ii) The points from $C \setminus S$ are closer to the origin than the points from $S \setminus C$. I.e., more formally: If $(u,v) \in S \setminus C$ and $(w,z) \in C \setminus S$ then $u^2+v^2 > w^2+z^2$ (see Fig. 1).

Further, (i) and (ii) give:

$$\iint_{S\setminus C} (x^2+y^2)\ dx\ dy \ \geq \ \iint_{C\setminus S} (x^2+y^2)\ dx\ dy. \tag{4}$$

Now, we prove (2):

$$\begin{aligned}
\mu_{2,0}(S)+\mu_{0,2}(S) &= \iint_S (x^2+y^2)dxdy \\
&= \iint_{S\setminus C} (x^2+y^2)dxdy + \iint_{S\cap C} (x^2+y^2)dxdy \\
&\geq \iint_{C\setminus S} (x^2+y^2)dxdy + \iint_{S\cap C} (x^2+y^2)dxdy \\
&= \iint_C (x^2+y^2)dxdy \ = \ \frac{\mu_{0,0}(S)^2}{2\pi}.
\end{aligned}$$

To prove (3), notice that both S and C are compact and $S \neq C$ implies that the inequality (4) is strict. So,

$$\mu_{2,0}(S)+\mu_{0,2}(S) > \mu_{2,0}(C)+\mu_{0,2}(C) = \frac{\mu_{0,0}(S)^2}{2\pi}$$

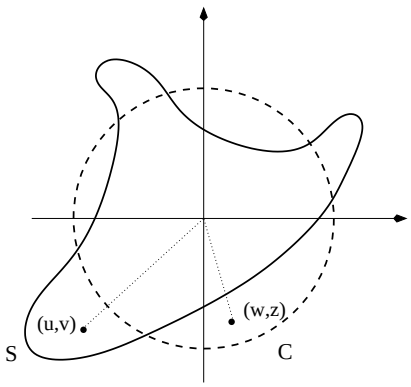

Figure 1: Each point (w,z) from $C \setminus S$ is closer to the origin than any point (u,v) from $S \setminus C$.

for all S different from a circle. This established the proof. □

Note. It is worth mentioning that the proof of Theorem 1 actually makes it intuitively clear why the quantity $\mu_{2,0}(S)+\mu_{0,2}(S)$ reaches its minimum for a circle, and thus, is suitable to be used for a circularity measure. From the proof (see also Fig. 1) it becomes clear that: If we would like to construct a shape S having the minimum possible value of $\mu_{2,0}(S)+\mu_{0,2}(S)$, then none of the points whose squared distance to the shape centroid is, let us say, d^2 may be included before all the points whose squared distance to the centroid of S is less than d^2 are already included in S. Roughly speaking, such a "greedy algorithm" (in this particular case) leads to a circle as the optimal (shape) solution of this optimization problem. □

Thus, Theorem 1 says that $(\mu_{2,0}(S) + \mu_{0,2}(S))/\mu_{0,0}(S)^2$ reaches its minimum if and only if S is a circle. This minimum is $1/(2\pi)$. Based on this, we give the following definition.

Definition 1 *Let S be a given shape. Then the circularity measure $\mathcal{C}(S)$ is defined as*

$$\mathcal{C}(S) = \frac{1}{2\pi} \cdot \frac{\mu_{0,0}(S)^2}{\mu_{2,0}(S) + \mu_{0,2}(S)}. \tag{5}$$

Theorem 2 summarises the desirable properties of $\mathcal{C}(S)$.

Theorem 2 *The circularity measure $\mathcal{C}(S)$ satisfies:*

(a) $\mathcal{C}(S) \in (0, 1]$, *for all shapes S;*

(b) $\mathcal{C}(S) = 1 \quad \Leftrightarrow \quad$ *S is a circle;*

(c) *$\mathcal{C}(S)$ is an invariant w.r.t. similarity transformations;*

(d) *For each $\delta > 0$ there is a shape S such that $0 < \mathcal{C}(S) < \delta$.*

Proof. Items (**a**) and (**b**) follow directly from Theorem 1.

Item (**c**) follows from the fact that the quantity $(\mu_{2,0}(S)+\mu_{0,2}(S))/\mu_{0,0}(S)^2$ is invariant with respect to similarity transformations. So, $\mu_{0,0}(S)^2/(2\pi(\mu_{2,0}(S)+\mu_{0,2}(S)))$ is also such an invariant.

To prove (**d**), let us consider a rectangle $T(t)$ whose edge lengths are 1 and t, where t is an arbitrary positive number. It is easy to verify that

$$\mathcal{C}(T(t)) = \frac{1}{2\pi}\cdot\frac{(\mu_{0,0}(T(t)))^2}{\mu_{2,0}(T(t))+\mu_{0,2}(T(t))} = \frac{6\cdot t}{\pi\cdot(t^2+1)}. \tag{6}$$

A trivial equality: $\lim_{t\to\infty}\mathcal{C}(T(t)) = 0$ completes the proof. □

Remark. Notice that the measured circularity $\mathcal{C}(T(t)) = 6t/(\pi\cdot(t^2+1))$ is in accordance with our perception. The highest measured circularity is for $t=1$; i.e., among all rectangles the square has the highest measured circularity. This is as expected. Also, when $t\to\infty$ and $t\to 0$ the measured circularity tends to 0. In those cases the rectangle degenerates into an infinitely long (but with constant width) strip ($t\to\infty$) or into a line segment ($t\to 0$), and such a measured circularity, tending to 0, seems to be very reasonable.

3 Experiments Illustrating $\mathcal{C}(S)$ Behaviour

Examples in Fig.2 illustrate how the new circularity measure acts. Ten fish shapes are ranked with respect to their measured $\mathcal{C}(S)$ circularity (the numbers given immediately below the shapes). It could be said that the obtained ranking is in accordance with our perception.

If the same shapes are ranked with respect to $\mathcal{C}_{st}(S)$, a different ranking $(b)(a)(c)(d)(e)(g)(h)(f)(i)(j)$ (instead of $(a)(b)(c)(d)(e)(f)(g)(h)(i)(j)$) is obtained. Such a different ranking is expected. The standard circularity measure $\mathcal{C}_{st}(S)$ penalises deep intrusions into the shape. Such intrusions lead to a perimeter increase and, consequently, implies a lower measured circularity. That is exactly what happened here. The shape in Fig.2(a) has a higher measured $\mathcal{C}(S)$ circularity than the shape in Fig.2(b). On the other hand, the measure $\mathcal{C}_{st}(S)$ penalises intrusions into the shape in Fig.2(a) and assigns a higher measured circularity $\mathcal{C}_{st}(S)$ to the shape in Fig.2(b). The same reasons lead to the 8th position of the shape in Fig.2(f) if ranked by $\mathcal{C}_{st}(S)$ measure.

Several more shapes are presented in Fig.3. The same reasoning applies. The biggest differences among the $\mathcal{C}(S)$ and $\mathcal{C}_{st}(S)$ rankings are in the case of shapes that have deep intrusions. Ranking $(a)(b)(c)(d)(e)(f)(g)(h)(i)(j)$ by $\mathcal{C}(S)$ is replaced by the ranking $(a)(c)(e)(f)(i)(b)(g)(h)(j)(d)$. A highly ranked shape in Fig.3(d), by a use of $\mathcal{C}(S)$, is ranked the last

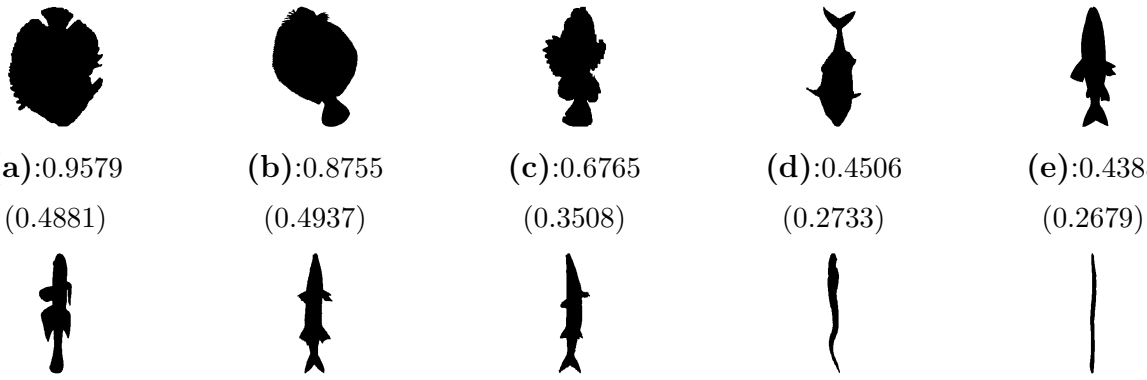

Figure 2: Fish shapes are ranked with respect to their measured $\mathcal{C}(S)$ circularities. Circularities measured by $\mathcal{C}_{st}(S)$ are in brackets.

if $\mathcal{C}_{st}(S)$ is applied. The examples in figures Fig.2(e) and Fig.2(f) (also in Fig.2(g) and Fig.2(h)) illustrate how shape deformations could lead to differences in the measured circularity. In both cases the changes in the measured circularity $\mathcal{C}(S)$ are in accordance with our perception of how a circularity measure should act – we prefer a higher circularity assigned to the shape in Fig.3(e) (Fig.3(g)) than for the shape in Fig.3(f) (Fig.3(h)).

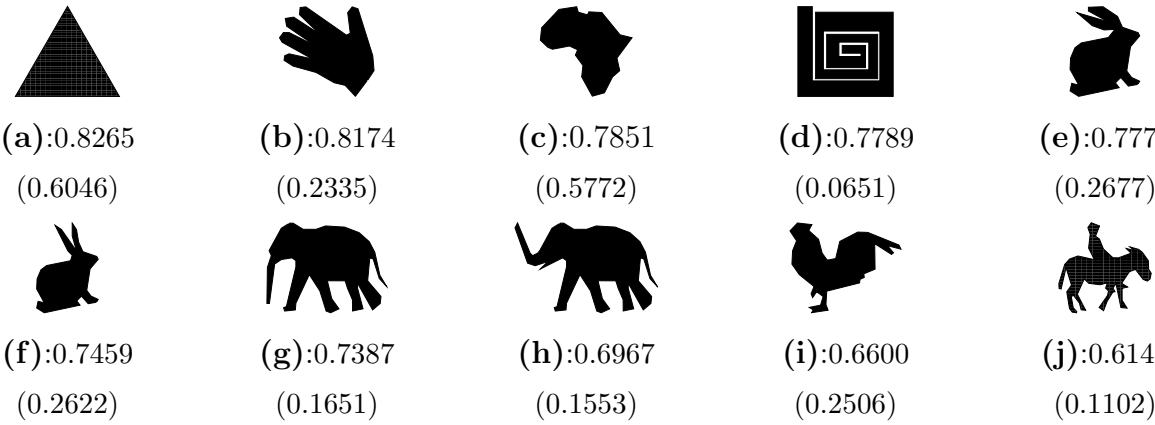

Figure 3: Shapes are ranked with respect to their measured $\mathcal{C}(S)$ circularities. Circularities measure by $\mathcal{C}_{st}(S)$ are in brackets.

Figure 4 illustrates that $\mathcal{C}(S)$ can be applied to compound objects as well. Three shapes consisting of three isometric circles are presented in Fig.4(a)-(c). In all three cases the standard circularity measure $\mathcal{C}_{st}(S)$ assigns the same measured circularity equal to $1/3 \approx 0.3333$. This is in accordance with formula (1), which, by the way, says that all compound

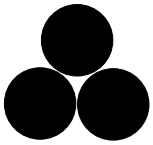

(a): 0.7909

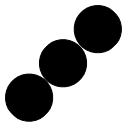

(b): 0.4540

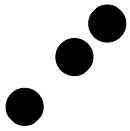

(c): 0.2091

Figure 4: Measured circularity $\mathcal{C}(S)$ of a compound shape S strongly depends on the mutual positions of the components of S.

object consisting of m isometric circles have the same assigned circularity $\mathcal{C}_{st}$ equal to $1/m$, independently on the mutual positions of the circles. On the other hand, the new measure strongly depends on such positions, and consequently assigns different circularity measures $\mathcal{C}(S)$ depending on them. The maximum circularity is measured when the circle centres are vertices of a regular triangle (Fig.4(a)), while the minimum circularity is measured when the disc centres belong to a line and circles are far away each other (Fig.4(c)). Such measured circularities match our expectation. This behaviour of $\mathcal{C}(S)$ in the case of compound objects can be considered to be an advantage over $\mathcal{C}_{st}(S)$.

Figure 5 illustrates the robustness of $\mathcal{C}(S)$. All four presented shapes have very similar measured $\mathcal{C}(S)$ circularities even though the fourth shape (in Fig.5(d)) has a very high noise level. On the other hand, the standard circularity measure $\mathcal{C}_{st}(S)$ can only cope with small levels of noise. Indeed, the shape in Fig.5(a) has approximately 2.3 times higher measured circularity than the shape in Fig.5(d).

(a):0.7470
(0.3155)

(b):0.7520
(0.3039)

(c):0.7565
(0.2289)

(d):0.7412
(0.1367)

Figure 5: Measured circularities $\mathcal{C}(S)$ of a shape with added noise. Measured $\mathcal{C}_{st}(S)$ circularities are in brackets.

4 Point Position Dependent Circularity Measure

In this section we further develop our approach in order to enable some control of the impact of the relative positions of points inside the shape on the computed circularity. Again, let S be a planar shape whose centroid coincides with the origin. Informally speaking, the quantity

$(\mu_{2,0}(S)+\mu_{0,2}(S))/\mu_{0,0}(S)^2$ can be understood as the average value of the squared distances of points from S to the centroid of S. Each point $(x,y)\in S$ contributes to $\mu_{2,0}(S)+\mu_{0,2}(S)$ by x^2+y^2. Obviously, such an impact is smaller if (x,y) is closer to the centroid of S. Since $\mathcal{C}(S)$ is proportional to the reciprocal value of $(\mu_{2,0}(S)+\mu_{0,2}(S))/\mu_{0,0}(S)^2$, we can say that points with a lower distance to the centroid of S have a bigger impact on the computed circularity measure of S. The question is: *Is such an impact of the position of points, with respect to the shape centroid, always suitable or would we like to change it in some particular situations?*

For example, if we consider the measured $\mathcal{C}(S)$ circularity of the fish in Fig.2(b), are we happy with the measured circularity $\mathcal{C}(S)$ which is 0.8755? Or, would we like to give a higher impact to the points which belong to the fish's tail (and which are away from the shape centroid) and, in such a way, reduce the measured circularity? Would we like to give a higher impact to the points closer to the shape centroid and, in such a way, reduce the impact of the rabbit's ears (see Fig.3(e) and Fig.3(f)) and, consequently, obtain more similar measured circularities for those rabbit shapes? In this section we give a modified method which allows us to control the impact of a point's position on the measured shape circularity.

We proceed with the following two lemmas which can be proven by using the approach from the proof of Theorem 1.

Lemma 1 *Let S be a given planar compact shape whose centroid coincides with the origin, and constant $\beta>0$. Then*

$$\frac{\iint_S (x^2+y^2)^\beta dxdy}{(\mu_{0,0}(S))^{\beta+1}} \geq \frac{1}{\pi^\beta(\beta+1)} \tag{7}$$

$$\frac{\iint_S (x^2+y^2)^\beta dxdy}{(\mu_{0,0}(S))^{\beta+1}} = \frac{1}{\pi^\beta(\beta+1)} \quad \Leftrightarrow \quad S \text{ is a circle.} \tag{8}$$

Proof. Similarly as in the proof of Theorem 1, we consider the circle C with radius $r=\sqrt{\mu_{0,0}(S)/\pi}$ (i.e. preserving $\mu_{0,0}(S)=\mu_{0,0}(C)$) and centred at the origin. Then (see Fig.1), because a positive β is assumed:

$$(u,v)\in S\setminus C,\ (w,z)\in C\setminus S \ \ \Rightarrow \ \ (u^2+v^2)^\beta > (w^2+z^2)^\beta,$$

which gives immediately:

$$\iint_{S\setminus C}(x^2+y^2)^\beta\ dx\ dy \ \geq \ \iint_{C\setminus S}(x^2+y^2)^\beta\ dx\ dy. \tag{9}$$

Now, we prove (7):

$$\begin{aligned} & \iint_S (x^2+y^2)^\beta \, dx \, dy \\ = & \iint_{S\setminus C} (x^2+y^2)^\beta \, dx \, dy + \iint_{S\cap C} (x^2+y^2)^\beta \, dx \, dy \\ \geq & \iint_{C\setminus S} (x^2+y^2)^\beta \, dx \, dy + \iint_{S\cap C} (x^2+y^2)^\beta \, dx \, dy \\ = & \iint_C (x^2+y^2)^\beta \, dx \, dy \; = \; \frac{\mu_{0,0}(S)^{\beta+1}}{\pi^\beta(\beta+1)}. \end{aligned}$$

To prove (8) is enough to notice that $S \neq C$ would imply that the inequality (9) is strict. Consequently, $S \neq C$ gives

$$\iint_S \left(x^2+y^2\right)^\beta \, dx \, dy \;\; > \;\; \iint_C \left(x^2+y^2\right)^\beta \, dx \, dy$$

for all shapes different from circles. □

Lemma 1 considers only $\beta > 0$, but it is also possible to consider negative β. To preserve the convergence of the integrals we assume $\beta > -1$. Notice that, contrary to the situation when $\beta > 0$, in the case of $-1 < \beta < 0$ and S is a circle, the quantity $\iint_S (x^2+y^2)^\beta dxdy/(\mu_{0,0}(S))^{1+\beta}$ reaches the maximal possible value. This maximal value is $1/(\pi^\beta(1+\beta))$. Taking this into account, the proof of the next lemma can be derived analogously to the proof of Lemma 1 and because of that it is omitted.

Lemma 2 *Let S be a given planar compact shape whose centroid coincides with the origin and let β be a constant such that $-1 < \beta < 0$. Then*

$$\frac{\iint_S (x^2+y^2)^\beta dxdy}{\mu_{0,0}(S)^{\beta+1}} \leq \frac{1}{(\beta+1)\pi^\beta} \tag{10}$$

$$\frac{\iint_S (x^2+y^2)^\beta dxdy}{\mu_{0,0}(S)^{\beta+1}} = \frac{1}{(\beta+1)\pi^\beta} \;\Leftrightarrow\; S \text{ is a circle.} \tag{11}$$

Now, by the arguments from Lemma 1 and Lemma 2 we give the following definition for a modified measure.

Definition 2 *Let S be a given shape whose centroid coincides with the origin and a real β such that $-1 < \beta$ and $\beta \neq 0$. Then the circularity measure $\mathcal{C}_\beta(S)$ is defined as*

$$\mathcal{C}_\beta(S) = \begin{cases} \dfrac{\mu_{0,0}(S)^{\beta+1}}{(\beta+1)\pi^\beta \iint_S (x^2+y^2)^\beta dxdy}, & \beta > 0 \\ \dfrac{(\beta+1)\pi^\beta \iint_S (x^2+y^2)^\beta dxdy}{\mu_{0,0}(S)^{\beta+1}}, & \beta \in (-1,0) \end{cases} \tag{12}$$

Definition 2 generalises Definition 1. Obviously, $\mathcal{C}_{\beta=1}(S) = \mathcal{C}(S)$. Also, Definition 2 allows control of the impact of the points' positions with respect to the centroid of S on the measured circularity $\mathcal{C}_\beta(S)$ by a suitable choice of β. This is illustrated by two synthetic examples in Fig.6. Irregularities from a perfect circle for the shape in Fig.6(a) are caused by the square gap that includes the shape centroid, while irregularities for the shape in Fig.6(b) are caused by the enclosing triangle. Let us consider $\beta > 0$. For $\beta \in (0, 1.447)$ the shape in Fig.6(b) has a greater measured circularity $\mathcal{C}_\beta(S)$ than the shape in Fig.6(b). For $\beta = 1.447$ both measured circularities are the same and equal to 0.6347. For $\beta > 1.447$ the measure $\mathcal{C}_\beta(S)$ gives the opposite ranking for those shapes and the shape in Fig.6(b) has a smaller measured circularity $\mathcal{C}_\beta(S)$ than the shape in Fig.6(a). Also the measured circularity of the

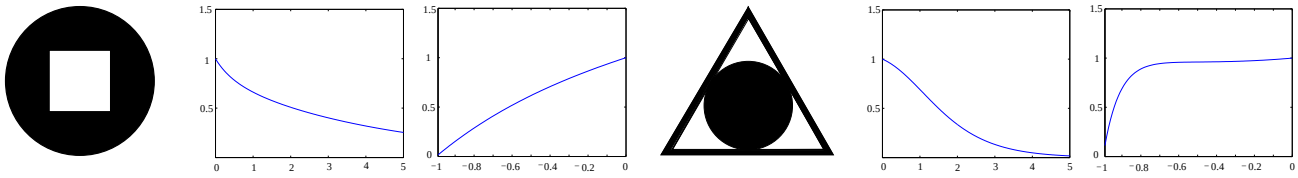

Figure 6: Graphs of the measured circularities $\mathcal{C}_\beta(S)$ (for the shapes (a) and (b)) for $\beta \in [0, 5]$ and $\beta \in (-1, 0]$ are displayed.

shape in Fig.6(b) converges much faster to zero (as β tends to infinity) (see Lemma 3, the equality (13)) than the measured circularity of the shape in Fig.6(a). That is as expected. In accordance with Definition 2 (see (12), $\beta > 0$), the impact of points belonging to the enclosing triangle in Fig.6(b), being distant from the shape centroid, strongly increases as β increases and leads to a fast decrease of the measured circularity. E.g., for $\beta = 5$ the measured circularity for the shape in Fig.6(b) is 0.0168 while the measured circularity for the shape in Fig.6(a) is much higher and equals 0.2538. Thus, a suitable choice of β could give a different ranking, depending on either $\beta \in (0, 1.447)$ or $\beta \in (1.447, \infty)$, among the shapes presented in Fig.6. Even more, a suitable choice of β could substantially increase the difference in the measured circularities of shapes in Fig.6(a) and Fig.6(b), which is good for classification purposes. The situation when $\beta \in (-1, 0)$ is analogous.

It is worth mentioning that such a generalised measure $\mathcal{C}_\beta(S)$ still keeps the basic requirements that each circularity measure should have. We give the following theorem which summarises the desirable properties of $\mathcal{C}_\beta(S)$. The proof is omitted because of the analogy with the proof of Theorem 2.

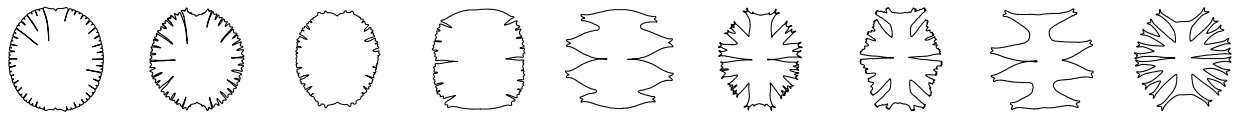

(a) (b) (c) (d) (e) (f) (g) (h) (i)

	$\beta = 1.0$	$\beta = -0.9$	$\beta = -0.5$	$\beta = 0.3$	$\beta = 1.2$	$\beta = 1.5$	$\beta = 2.0$	$\beta = 5$	$\beta = 10$
(a)	0.9910	0.7949	0.9984	0.9981	0.9883	0.9837	0.9748	0.8943	0.7030
(b)	0.9819	0.7565	0.9965	0.9961	0.9767	0.9681	0.9516	0.8167	0.5440
(c)	0.9817	0.7469	0.9969	0.9963	0.9760	0.9664	0.9475	0.7789	0.4418
(d)	0.9763	0.9143	0.9977	0.9950	0.9695	0.9581	0.9367	0.7650	0.4520
(e)	0.9084	0.7392	0.9823	0.9786	0.8848	0.8478	0.7832	0.4234	0.1119
(f)	0.8822	0.7999	0.9788	0.9729	0.8514	0.8028	0.7182	0.2818	0.0309
(g)	0.8443	0.8052	0.9712	0.9633	0.8053	0.7449	0.6435	0.1979	0.0158
(h)	0.7408	0.8327	0.9526	0.9355	0.6829	0.5989	0.4722	0.0855	0.0026
(i)	0.7396	0.7653	0.9509	0.9355	0.6806	0.5945	0.4637	0.0746	0.0022

Figure 7: Examples of *Micrasterias* desmid shapes and their measured $\mathcal{C}_\beta(S)$ convexities for $\beta = 1.0, -0.9, -0.5, 0.3, 1.2, 1.5, 2.0, 5.0, 10.0$. $\mathcal{C}_\beta(S)$ was calculated on the boundary and interior of S, but only the boundaries are displayed here so as to better highlight the many narrow intrusions of the shapes.

Theorem 3 *Let β be a real number, such that $\beta \neq 0$ and $\beta > -1$. Then, the circularity measure $\mathcal{C}_\beta(S)$ satisfies the following properties:*

(a) $\mathcal{C}_\beta(S) \in (0, 1]$ *for all planar shapes S;*

(b) $\mathcal{C}_\beta(S) = 1 \quad \Leftrightarrow \quad S$ *is a circle;*

(c) $\mathcal{C}_\beta(S)$ *is invariant w.r.t. the similarity transformations;*

(d) *For each $\delta > 0$ there is a shape S such that $0 < \mathcal{C}_\beta(S) < \delta$.*

More examples are given in Fig.7. Nine microorganism shapes are listed in accordance with their $\mathcal{C}(S) = \mathcal{C}_{\beta=1}(S)$ measured circularity (see the second column in the table in Fig.7). The modified circularities are also computed for $\beta = -0.9, -0.5, 0.3, 1.2, 1.5, 2.0, 5.0, 10.0$. It can be seen that $\beta = -0.5$, $\beta = 0.3$ and $\beta = 10$ give slightly different rankings while $\beta = -0.9$ gives an essentially different ranking, which can be exploited in particular classification tasks. Notice that for a relatively small β (e.g. $\beta = 1.0$, $\beta = 1.2$ or $\beta = 1.5$), the circularity measure $\mathcal{C}_\beta(S)$ does not strongly distinguish between the shapes in Fig.7(a)-(d) while a large $\beta = 10$

(and even $\beta = 5.0$) does not strongly distinguish between shapes in Fig.7(f)-(i). Overall, it could be said that, for those particular shapes given in Fig.7, the best choice, in terms of "classification separability", would be $\beta = 2$.

Looking again at Fig.7 it can be seen that for a high β (e.g. $\beta = 10$) the measured circularity for shapes in Fig.7(f)-(i) dramatically decreases to zero. Those shapes strongly differ from a perfect circle. For shapes which could be understood as "nearly circular" their measured circularities $\mathcal{C}_{\beta=10}(S)$ are still reasonably high. That is in accordance with the theoretical considerations. We give the following lemma which describes the behaviour of $\mathcal{C}_\beta(S)$ when β is large, or formally, when β tends to infinity. For completeness, the lemma also considers the trivial case $\beta \to 0$. It is easily seen that $\mathcal{C}_{\beta=0}(S) = 1$ for all shapes (this directly follows from Definition 2). That is in accordance with examples in given in Fig.7 and their computed circularities for $\beta = 0.3$. Indeed, all values are high and very close to 1.

Lemma 3 *For a planar compact shape S different from a circle*[1] *the following equalities hold:*

$$\lim_{\beta\to\infty} \mathcal{C}_\beta(S) \;=\; 0, \tag{13}$$

$$\lim_{\beta\to 0} \mathcal{C}_\beta(S) \;=\; \mathcal{C}_{\beta=0}(S) \;=\; 1. \tag{14}$$

Proof. The proof the equality (14) follows directly from the definition (see (12)). The proof of (13) follows.

Let S be a given planar compact shape different from a circle and let C be the circle with radius $r_C = \sqrt{\mu_{0,0}(S)/\pi}$ (providing $m_{0,0}(S) = m_{0,0}(C)$), and centre coincident with the centroid of S. Because S and C are compact and $S \neq C$ we have

$$\Delta \;=\; \mu_{0,0}(S \setminus C) \;=\; \mu_{0,0}(C \setminus S) \;>\; 0. \tag{15}$$

Also, let

$$r_{ext} = \sqrt{(\mu_{0,0}(S) + \Delta)/\pi} \tag{16}$$

providing that:

(a) the circular ring determined by the circles, centred at the centroid of S, and having radii r_C and r_{ext} has the area Δ. (Notice: $r_C < r_{ext}$.)

Now, by applying the same reasoning as in the proof of Theorem 1, assuming $\beta > 1$, and by using **(a)** and (16) we have:

[1] If S is a circle then $\mathcal{C}_\beta(S)$ is identically equal to 1 for all $\beta > -1$, and consequently $\lim_{\beta\to\infty} \mathcal{C}_\beta(S) = \lim_{\beta\to 0} \mathcal{C}_\beta(S) = 1$.

$$\iint\limits_{S\setminus C}(x^2+y^2)^\beta\ dx\ dy \geq \iint\limits_{r_C\leq\sqrt{x^2+y^2}\leq r_{ext}}(x^2+y^2)^\beta dxdy$$

$$= \frac{\pi}{\beta+1}\left(\frac{\mu_{0,0}(S)+\Delta}{\pi}\right)^{\beta+1} - \frac{\pi}{\beta+1}\left(\frac{\mu_{0,0}(S)}{\pi}\right)^{\beta+1}$$

$$= \frac{\pi}{\beta+1}\left(\frac{\mu_{0,0}(S)}{\pi}\right)^{\beta+1}\left(\left(1+\frac{\Delta}{\mu_{0,0}(S)}\right)^{\beta+1}-1\right)$$

(Taylor expansion implies an $\omega\in(0,1)$)

$$= \frac{\mu_{0,0}(S)^{\beta+1}}{(\beta+1)\pi^\beta}\left(\frac{(\beta+1)\Delta}{\mu_{0,0}(S)} + \frac{(\beta+1)\beta\Delta^2}{2\mu_{0,0}(S)^2}\left(1+\omega\frac{\Delta}{\mu_{0,0}(S)}\right)^{\beta-1}\right)$$

$$> \frac{\mu_{0,0}(S)^{\beta+1}}{(\beta+1)\pi^\beta}\frac{\Delta}{\mu_{0,0}(S)}(\beta+1) = \frac{\mu_{0,0}(S)^\beta\Delta}{\pi^\beta}. \tag{17}$$

Further, (17) gives

$$\iint_S(x^2+y^2)^\beta\ dx\ dy > \iint_{S\setminus C}(x^2+y^2)^\beta dxdy$$

$$> \frac{\mu_{0,0}(S)^\beta\Delta}{\pi^\beta}. \tag{18}$$

Finally,

$$\mathcal{C}_\beta(S) = \frac{1}{(\beta+1)\pi^\beta}\cdot\frac{\mu_{0,0}(S)^{\beta+1}}{\iint_S(x^2+y^2)^\beta\ dx\ dy} < \frac{\mu_{0,0}(S)}{(\beta+1)\cdot\Delta}. \tag{19}$$

Taking into account that Δ is strictly positive and does not depend on β, (19) gives immediately the required equality $\lim\limits_{\beta\to\infty}\mathcal{C}_\beta(S) = 0$ which holds for each shape S different from a circle. □

Examples given in Fig.8 illustrate that $\mathcal{C}_\beta(S)$, for a large β, strongly penalises deviations of S from a perfect circle. Indeed, the shape in Fig.8(a), being a regular 14-gon, is very similar to a perfect circle. Its measured circularity decreases slowly on the interval $[0,20]$. The shape in Fig.8(b) is a regular 7-gon and differs more than the 14-gon from a perfect circle. Such a greater difference is strongly penalised by $\mathcal{C}_\beta(S)$ which decreases much faster to 0 as β increases. The next two shapes in Fig.8(c) and Fig.8(d) are circles with added noise on their boundaries. In the case of a small amount of added noise (Fig.8(c)), there is a slight decrease of $\mathcal{C}_\beta(S)$ on the interval $[0,20]$, while in the case of high noise levels such a decrease is much faster (Fig.8(d)). Two circles with added 2% and 10% "salt noise" are given in Fig.8(e) and Fig.8(f). The change in the speed of the decrease, as a function of the noise level, is obvious from the presented graphs.

All shapes in Fig.8(a)-(f) could understood as pretty much nearly circular and depending on their irregularities it is necessary to set a β large enough to be able to detect their

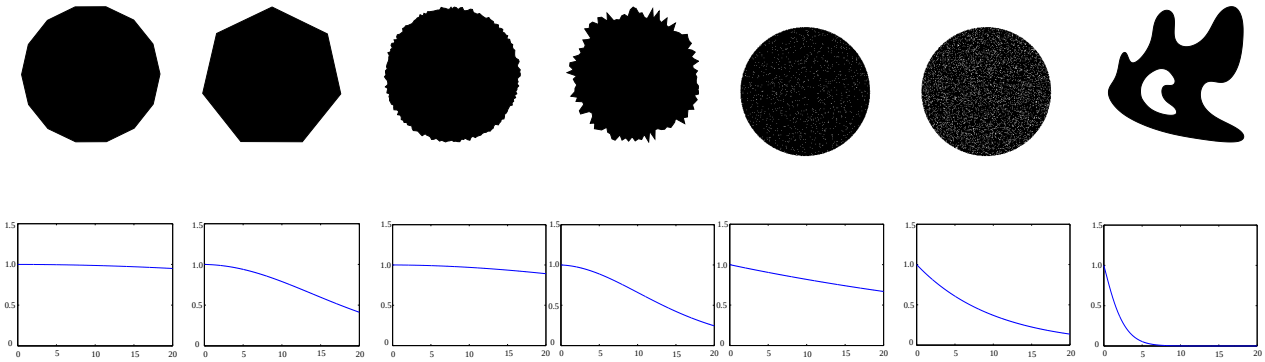

(a) (b) (c) (d) (e) (f) (g)

Figure 8: Graphs of the measured circularities $\mathcal{C}_\beta(S)$, for $\beta \in [0, 20]$, are given below the corresponding shapes.

deviations from a perfect circle by a use of $\mathcal{C}_\beta(S)$. In the case of shapes in Fig.8(a), Fig.8(c), and Fig.8(e) such a β should be large (say $\beta = 20$), while in the cases of the shapes in Fig.8(b), Fig.8(d), and Fig.8(f), a much smaller β, say $\beta = 5$, will do. The shape in Fig.8(g) is given as an illustration that for irregular shapes, very different from a perfect circle, use of a very big β does not make sense because the measured circularity $\mathcal{C}_\beta(S)$ very quickly converges to zero.

5 An Application to Measuring Shape Linearity

In this section we will illustrate that a shape linearity measure can be obtained as a "by-product" from the new circularity measure $\mathcal{C}(S)$. At first instance, it could seem reasonable that shapes with a very low measured circularity are expected to be more linear. E.g., if we consider the standard circularity measure $\mathcal{C}_{st}(S)$ such a hypothesis is valid for the shapes given in Fig.2(i) and Fig.2(j). The measured circularities $\mathcal{C}_{st}(S)$ are 0.1545 and 0.0982 and if we use the quantities computed as $1 - \mathcal{C}_{st}(S)$, the obtained values 0.8455 and 0.9018 seem to be very reasonable as the corresponding linearity measures for the shapes. But the hypothesis that $1 - \mathcal{C}_{st}(S)$ can be used effectively as a linearity measure collapses in the case of the shape in Fig.3(d). Indeed, the linearity measure assigned in such a way would be 0.9349 which is very high, and, because of that, unacceptable. On the other hand, in the case of the circularity measure $\mathcal{C}(S)$ derived here, the quantity $1-\mathcal{C}(S)$ behaves more consistently. For the "very linear" shapes in Fig.2(i) and in Fig.2(j) it assigns 0.8610 and 0.9271 as very

acceptable measured shape linearity values. In the case of the shape in Fig.3(d), the assigned linearity $1 - \mathcal{C}(S)$ is low and equal to an acceptable 0.2211. Moreover, if we consider the compound shapes in Fig.4(a)-(c), then the assigned linearity values, measured by $1 - \mathcal{C}(S)$, would be 0.2091, 0.5460, and 0.7909 which seems acceptable. Of course, the same linearity (equal to 2/3), assigned to all the shapes in Fig.4 by a use of $1 - \mathcal{C}_{st}(S)$, is unacceptable.

More examples are given in Fig.9. Shapes are listed in accordance with their linearity measure computed as $1 - \mathcal{C}(S)$. Such a ranking seems reasonable. On the other hand, the linearity measure $1-\mathcal{C}_{st}(S)$, derived from the standard circularity measure, gives the ranking

(a):0.9133 **(b)**:0.8681 **(c):**0.8417 **(d)**:0.7676 **(e)**:0.7079 **(f)**:0.6928 **(g)**:0.5296 **(h)**:0.4965
(0.9009) (0.8529) (0.8312) (0.8725) (0.8836) (0.8572) (0.9556) (0.8785)

Figure 9: Shape linearities measured by $1 - \mathcal{C}(S)$ are immediately below the shapes. Shape linearity values measured by $1 - \mathcal{C}_{st}(S)$ are in brackets.

$(g)(a)(e)(h)(d)(f)(b)(c)$ which is not acceptable. Indeed, the highest linearity assigned to the shape in Fig.9(g) and the lowest linearity assigned to the shape in Fig.9(c) do not match our expectation.

6 Applications of Circularity

Since $\mathcal{C}(S)$ has been shown to measure both the circularity and linearity of shapes in a reasonable manner it can be expected that it should be suitable for use in applications such as classification tasks. Moreover, the addition of position dependency in $\mathcal{C}_\beta(S)$ expands the set of available shape measures. In this section several examples of applications are given for the proposed circularity measure as well as $\mathcal{C}_{st}(S)$ and the circularity measures of Proffitt [20] and Haralick [9]. For $\mathcal{C}_{st}(S)$ perimeter was calculated either directly from the pixel boundaries extracted from the images with inter-pixel weights set according to Dorst and Smeulders [5]; as an alternative, the perimeters were calculated from polygonal approximations of the boundaries [22]. For classification, leave one out testing was performed with a nearest neighbour classifier using Euclidean distances.

For the first example, circularity was measured for the set of 54 masses from mammograms, combining images from the MIAS and Screen Test databases [23], see Fig.10. Ran-

circularity	mammography			galaxy	print
measure	circ./spic.	mal./ben.	4 groups		quality
$\mathcal{C}_{\beta=1/8}(S)$	83.33	66.67	51.85	77.88	0.483
$\mathcal{C}_{\beta=1/4}(S)$	85.19	64.81	51.85	78.85	0.485
$\mathcal{C}_{\beta=1/2}(S)$	75.93	57.41	42.59	79.81	0.488
$\mathcal{C}_{\beta=1}(S)$	68.52	68.52	51.85	75.96	0.492
$\mathcal{C}_{\beta=2}(S)$	75.93	68.52	53.70	75.96	0.493
$\mathcal{C}_{\beta=4}(S)$	72.22	46.30	33.33	80.77	0.481
$\mathcal{C}_{\beta=8}(S)$	79.63	59.26	50.00	79.81	0.444
$\mathcal{C}_{\beta=16}(S)$	87.04	57.41	51.85	84.62	0.363
$\mathcal{C}_{\beta=32}(S)$	**90.74**	**70.37**	**64.81**	83.65	0.152
$\mathcal{C}_{st}(S)$ pix.	87.04	59.26	57.41	83.65	0.539
$\mathcal{C}_{st}(S)$ pol.	85.19	59.26	57.41	**85.58**	**0.575**
Haralick [9]	68.52	46.30	37.04	79.81	0.447
Proffitt [20]	51.85	42.59	25.93	76.92	0.401

Table 1: Applications of the circularity measures to: classification of mammographic masses; classification of galaxy morphologies; and determination of print quality (mottling). The first four columns of results report classification accuracies and the final column shows correlation coefficients. Results for the best performing measure for each task is highlighted in bold.

CB CM SB SM

Figure 10: Examples of the four classes of mammographic masses: circumscribed benign (CB), circumscribed malignant (CM), spiculated benign (SB), spiculated malignant (SM). The masses were extracted from the mammograms on the left, and have been drawn rescaled.

Figure 11: Galaxy images with their shapes extracted by thresholding. The two galaxies on the left are spiral while those on the right are elliptical.

gayyan *et al.* [23] assessed the measures by classifying them as circumscribed/spiculated, benign/malignant, and CB/CM/SB/SM, in two group and four group classification experiments. Their best shape measure results for the three classification tasks were: 1/ circumscribed versus spiculated: 88.9% achieved by both $\mathcal{C}_{st}(S)$ and a Fourier based shape factor, 2/ benign versus malignant: 75.9% achieved by the Fourier based shape factor, 3/ four-way discrimination: 64.8% achieved by both $\mathcal{C}_{st}(S)$ and the Fourier based shape factor.[2] From table 1 we see that the best results from using $\mathcal{C}_{\beta}(S)$ occurred for $\beta = 32$ and were respectively better, worse, and equal to Rangayyan *et al.*'s. The other circularity measures did not perform as well as $\mathcal{C}_{\beta}(S)$.

The second task was to classify galaxies into two morphological groups: spiral and elliptical. The data consisted of 104 100×100 images. The original classification by Lekshmi *et al.* [16] used a fractal signature, and achieved accuracies of 92.3% and 95.1% using nearest neighbour and neural network classifiers respectively. In this paper we restrict analysis to binary shape data, and threshold the images as shown in Fig.11. Classification with just one circularity value is unable to reach the same level of accuracy as using the image texture, but reasonable results are still obtained. The accuracy for $\mathcal{C}_{\beta=16}(S)$ is significantly above the Proffitt and Haralick circularity accuracies (see table 1). Compared to $\mathcal{C}_{st}(S)$ it was slightly above or below its accuracy, depending on how perimeter was computed.

The third example was print quality evaluation, in which quality assessment is carried out by measuring mottling (unevenness of print) by analysis of dots from images of halftoning [6]. The data set consists of 20 images (size 2000×2000 pixels), each containing approximately 55000 dots. In addition, the images were evaluated by experts, providing a set of mottling indices which were used for groundtruthing. Figure 12(a) shows a small portion cropped from one of the images; since the printed dots touch each other the image has been inverted (as in [6]) so that the gaps will be analysed instead of the dots themselves. The image was

[2]We note that our results for $\mathcal{C}_{st}(S)$ listed in table 1 do not match Rangayyan *et al.*'s [23] reported accuracies for $\mathcal{C}_{st}(S)$. This can be attributed to several factors: 1/ different classifiers were used, and also 2/ different methods for estimating perimeter may have used.

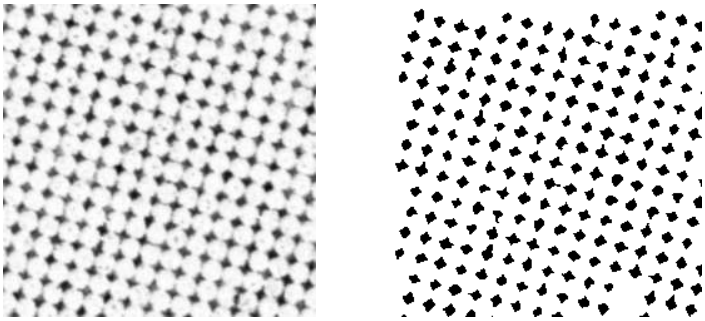

(a) (b)

Figure 12: A small portion of a printed dot pattern before and after thresholding and removal of outsized dots.

thresholded using the RATS algorithm [34] to allow for non-uniformity of illumination, and blobs touching the image boundaries (in the cropped image in Fig.12(a) this corresponds to the top and left boundaries only) and overly small or large blobs (which generally resulted from faulty thresholding) were removed – see Fig.12(b). The effectiveness of the circularity measures as a predictor of mottling was determined by computing Pearson's correlation coefficient between the circularity measures and the human mottling indices. The correlation values of the single circularity measures are shown in table 1. It can be seen that $\mathcal{C}_{st}(S)$ applied to the polygonal approximation of the boundary data considerably outperformed all the other circularity measures. However, using $\mathcal{C}_\beta(S)$ we can also combine a set of circularities with different values of β to provide a more effective composite measure. In [6] a linear combination of a set of miscellaneous shape measures was built from a subset of the data, and they were able to achieve a correlation coefficient of 0.72. We apply a similar approach, and use half the image data to estimate the weights for the linear combination of the set of nine $\mathcal{C}_\beta(S)$ values to best match the human mottling indices, where the nine β values are given in table 1. Using these weights the average correlation coefficient, obtained from the combination of nine $\mathcal{C}_\beta(S)$ values generated from the remainder of the image data, was 0.77 which compares favourably to [6].

7 Conclusion

We have shown in this paper that the well known Hu moment invariant $(\mu_{2,0}(S)+\mu_{0,2}(S))/\mu_{0,0}(S)^2$ reaches its minimum value if and only if S is a circle. We note that, to the best of the authors' knowledge, that is the first of such results, and it is not known yet whether similar

statements hold for other Hu invariants. This remains an open problem for further research. Exploiting the fact that circles maximize the above invariant has enabled us to introduce a new circularity measure $\mathcal{C}(S)$ defined as in (5). It is shown that $\mathcal{C}(S)$ ranges over the interval $(0, 1]$ and that $\mathcal{C}(S)$ equals 1 if and only if S is a perfect circle. Also, $\mathcal{C}(S)$ is invariant with respect to rotations, translations and scaling. Being an area based measure, $\mathcal{C}(S)$ is robust – e.g. with respect to a noise or narrow intrusions. The behaviour of $\mathcal{C}(S)$ is demonstrated on illustrative examples.

Such a defined $\mathcal{C}(S)$ measure enables an easy and straightforward estimation since only up to second order moments are required. Note that, taking into account that in real applications we are working with digital images (i.e. discrete data), an exact computation of $\mathcal{C}(S)$ is not possible – we can have only approximated values with the accuracy dependent on the available image resolution [14]. A straightforward and very accurate estimation (see [14] for the estimation efficiency) of moments $\mu_{p,q}(S)$ from the corresponding binary images can be done in $\mathcal{O}(r^2)$ time, if r denotes the applied image resolution (i.e. the number of pixels per measure unit). Indeed, it is enough to notice that a shape S presented on a binary image having resolution r consists of no more than $\mathcal{O}(r^2)$ pixels and use the approximation

$$m_{p,q}(S) \;=\; \iint_S x^p y^q dxdy \approx \sum_{pixel\ (i,j)\ is\ in\ S} i^p \cdot j^q.$$

But there are already well-known techniques (e.g. [17]) for fast computation of shape moments. In general, the geometric moments $\mu_{p,q}(S)$, of a given planar shape S can be computed from the boundary of S. Consequently, assuming that the order $p+q$ is bounded, an efficient estimation of $\mu_{p,q}(S)$ is possible in $\mathcal{O}(r)$ time. It is obvious that a better time complexity could not be reached if the circularity is measured by the standard circularity measure $\mathcal{C}_{st}(S)$. Of course, depending on which algorithm is used for the estimation of $perimeter\_of\_S$, the required complexity could be even higher. A similar complexity analysis could be done for $\mathcal{C}_\beta(S)$.

A detailed analysis of $\mathcal{C}(S)$ has shown that the shape points which are closer to the shape centroid have a bigger impact on the measured shape circularity. In order to be able to control the impact of the relative positions of points (inside the shape) on the measured shape circularity a modification of the $\mathcal{C}(S)$ measure is proposed by Definition 2. The choice of the parameter β, controls the impact of the shape points (depending on their distance to the shape centroid) to the computed $\mathcal{C}_\beta(S)$ measure. To illustrate such a behaviour of $\mathcal{C}_\beta(S)$ two synthetic and several real examples are given. Desirable properties of $\mathcal{C}_\beta(S)$ are proven. In addition, it has been shown that $\lim_{\beta\to\infty} \mathcal{C}_\beta(S) = 0$ for all shapes different from a circle. The

proven convergence of $\mathcal{C}_\beta(S)$ for non-circular shapes, when β increases, is useful and can be used for detecting irregularities in circular shapes damaged by noise or during an extraction process in practical image processing tasks. That is verified with several examples.

It turns out that the circularity measure $\mathcal{C}(S)$ behaves very consistently in the case of very low measured circularity (i.e. when the measured circularity is close to 0). Shapes with very low measured circularity $\mathcal{C}(S)$ appear to match our perception about shapes that should have a high linearity value estimated. This suggests that $1-\mathcal{C}(S)$ could be used as a linearity measure. The suitability of using $1-\mathcal{C}(S)$ as a shape linearity measure is illustrated by several examples.

Finally, several fairly recent image processing applications, covering a wide range (medical, industrial, astronomical), are given. Our comparative evaluation is restricted to scalar shape descriptors (which are generally simpler and, very often, more computationally efficient than more complex matching schemes). The proposed circularity measure is shown to perform better in several cases than the state of the art. In other cases it is outperformed by other measures – this is to be expected since no single shape measure will be universally superior than others for all applications.

Acknowledgements

We would like to thank Rangaraj M. Rangayyan for providing the mammographic data, Professors Revathy and Nayar for providing the galaxy images, Joni Kamarainen and Tuomas Eerola for providing the print quality evaluation data, and Michael Wilkinson for his RATS thresholding code. The work (the first author) is partially supported by the Serbian Ministry of Science of through the project ON144018 of the Mathematical Institute of the Serbian Academy of Science and Arts.

References

[1] L. Boxer. Computing deviations from convexity in polygons. *Pattern Recognition Letters*, **14**:163–167, 1993.

[2] E. Bribiesca. An easy measure of compactness for 2D and 3D shapes. *Pattern Recognition,* **41**:543-554, 2008.

[3] S. Derrode, F. Ghorbel. Shape analysis and symmetry detection in gray-level objects using the analytical Fourier-Mellin representation. *Signal Proc.,* **84**:25-39, 2004.

[4] C. Di Ruberto, A. Dempster. Circularity measures based on mathematical morphology. *Electronics Letters,* **38**:1691-1693, 2000.

[5] L. Dorst and A.W.M. Smeulders. Length estimators for digitized contours. *Computer Vision, Graphics and Image Processing*, **40**:311–333, 1987.

[6] T. Eerola, J.-K. Kamarainen, L. Lensu, and H. Kälviäinen. Visual print quality evaluation using computational features. In *Proc. Advances in Visual Computing, Part I*, *LNCS*,**4841**:403–413, 2007.

[7] J. Flusser, T. Suk. Pattern recognition by affine moment invariants. *Pattern Recognition,* **26**:167-174, 1993.

[8] V.H.S. Ha, J.M.F. Moura. Afine-permutation invariance of 2-D shape. *IEEE Trans. Image Processing,* **14**:1687-1700, 2005.

[9] R.M. Haralick. A measure for circularity of digital figures. *IEEE Transactions on Systems, Man and Cybernetics*, **4**:394–396, 1974.

[10] M. Hu. Visual pattern recognition by moment invariants. *IRE Trans. Inf. Theory*, **8**:179–187, 1962.

[11] R. Kakarala. Testing for convexity with Fourier descriptors. *Electronics Letters*, **34**:1392–1393, 1998.

[12] C.E. Kim, T.A. Anderson. Digital disks and a digital compactness measure. Proc. of the sixteenth annual ACM symposium on Theory of STOC 1984: 117-124.

[13] W.-Y. Kim, Y.-S. Kim. Robust rotation angle estimator. *IEEE Trans. Patt. Anal. Mach. Intell.,* **21**:768-773, 1999.

[14] R. Klette, I. Stojmenović, J. Žunić. Digital Approximation of Moments of Convex Regions. *Graphical Models and Image Processing,* **61**:274-298, 1999.

[15] D.R. Lee and T. Sallee. A method of measuring shape. *Geographical Review,* **60**:555-563, 1970.

[16] S. Lekshmi, K. Revathy, and S.R. Prabhakaran Nayar. Galaxy classification using fractal signature. *Astronomy and Astrophysics*, **405**:1163–1167, 2003.

[17] J.-G. Leu. Computing a shape's moments from its frontier. *Pattern Recognition*, **24**:949-957, 1991.

[18] H.B. Lin, J. Si, G.P. Abousleman. Orthogonal rotation-invariant moments for digital image processing. *IEEE Trans. Image Processing,* **17**:272-282, 2008.

[19] R.R. Martin, P.L. Rosin. Turning shape decision problems into measures. *Int. J. Shape Modelling*, **10**:83–113, 2004.

[20] D. Proffitt. The measurement of circularity and ellipticity on a digital grid. *Pattern Recognition*, **15**:383–387, 1982.

[21] E. Rahtu, M. Salo, J. Heikkila. A new convexity measure based on a probabilistic interpretation of images. *IEEE Trans. Patt. Anal. Mach. Intell.* **28**:1501-1512, 2006.

[22] U. Ramer. An iterative procedure for the polygonal approximation of plane curves. *Computer Graphics and Image Processing*, **1**:244-256, 1972.

[23] R.M. Rangayyan, N.M. Elfaramawy, J.E.L. Desautels, and O.A. Alim. Measures of acutance and shape for classification of breast-tumors. *IEEE Transactions on Medical Imaging*, **16**:799-810, 1997.

[24] P.L. Rosin. Measuring shape: ellipticity, rectangularity, and triangularity. *Machine Vision and Applications*, **14**:172-184, 2003.

[25] P.L. Rosin. Measuring sigmoidality. *Pattern Recognition*, **37**:1735-1744, 2004.

[26] P.L. Rosin, C.L. Mumford. A symmetric convexity measure. *Computer Vision and Image Understanding*, **103**:101–111, 2006.

[27] D. Shen, H.H.S. Ip. Generalized affine invariant normalization. *IEEE Trans. Patt. Anal. and Mach. Intell.,* **19**:431-440, 1997.

[28] D. Shen, H.H.S. Ip, K.K.T. Cheung, E.K. Teoh. Symmetry detection by generalized complex (GC) moments: A close-form solution. *IEEE Trans. Patt. Anal. Mach. Intell.,* **21**:466-476, 1999.

[29] M. Sonka, V. Hlavac, R Boyle,: *Image Processing, Analysis, and Machine Vision* Chapman and Hall, 1993.

[30] M. Stojmenović, A. Nayak. Shape based circularity measures of planar point sets. In *Proc. IEEE ICSPC*, pp. 127-1282, 2007.

[31] M. Stojmenović, A. Nayak J. Žunić. Measuring linearity of planar point sets. *Pattern Recognition*, **41**:2503-2511, 2008.

[32] M. Stojmenović, J. Žunić. Measuring elongation from shape boundary. *Journal Mathematical Imaging and Vision*, **30**:73-85, 2008.

[33] W.H. Tsai and S.L. Chou. Detection of generalized principal axes in rotationally symmetric shapes. *Pattern Recognition*, **24**:95-104, 1991.

[34] M.H.F. Wilkinson. Optimizing edge detectors for robust automatic threshold selection: Coping with edge curvature and noise. *Graphical Models and Image Processing*, **60**:385-401, 1998.

[35] D. Xu and H. Li. Geometric moment invariants. *Pattern Recognition*, **41**:240-249, 2008.

[36] J. Žunić, P.L. Rosin. Rectilinearity measurements for polygons. *IEEE Trans. Patt. Anal. and Mach. Intell.*, **25**:1193-1200, 2003.

[37] J. Žunić, P.L. Rosin. A new convexity measurement for polygons. *IEEE Trans. Pattern Analysis and Machine Intelligence*, **26**:923-934, 2004.

[38] J. Žunić, P.L. Rosin, L. Kopanja. On the orientability of shapes. *IEEE Trans. Image Processing*, **15**:3478-3487, 2006.